Exp Fluids (2016) 57:28
DOI 10.1007/s00348-016-2121-0

RESEARCH ARTICLE

Schlieren imaging of viscous fingering in a horizontal Hele-Shaw cell

P. Bunton[1] · D. Marin[1] · S. Stewart[1] · E. Meiburg[2] · A. De Wit[3]

Received: 24 August 2015 / Revised: 9 January 2016 / Accepted: 11 January 2016

Abstract Interfaces between different fluids can be unstable with regard to hydrodynamic instabilities such as viscous fingering or buoyancy-driven convection. To study such instabilities experimentally for transparent fluids, dyes or chemical indicators are most often used to track the dynamics. While the interfacial deformation can easily be tracked by color changes, it is difficult to have access to the internal flow structure for comparison with theoretical predictions. To overcome this problem, a modification of a Schlieren technique is introduced to image 3D flows during viscously driven instabilities in a horizontal Hele-Shaw cell without using any dye or chemical indicator. The method is exquisitely sensitive, readily yielding information about 3D flows in gaps under a millimeter and allowing imaging of the flow structure internal to the fingers, rather than merely imaging the flow boundary. Following a description of the technique, visualization of dynamics for nonreactive water–glycerol and reactive displacements is presented revealing previously unobserved internal flows. These flows are tentatively interpreted in terms of known theoretical predictions.

Electronic supplementary material The online version of this article (doi:10.1007/s00348-016-2121-0) contains supplementary material, which is available to authorized users.

✉ P. Bunton
buntonp@william.jewell.edu

[1] Department of Physics, William Jewell College, 500 College Hill, Liberty, MO 64068, USA

[2] Department of Mechanical Engineering, University of California at Santa Barbara, Santa Barbara, CA 93106, USA

[3] Nonlinear Physical Chemistry Unit, Service de Chimie Physique et Biologie Théorique, Université libre de Bruxelles (ULB), Campus Plaine, CP 231, 1050 Brussels, Belgium

1 Introduction

Flows through porous media are ubiquitous and affect pollution dispersal, enhanced petroleum recovery, chromatographic separation, packed bed reactors, aquifers, and highway drainage, to name a few. Since such media are often opaque, analyzing experimentally the flow dynamics and possible instabilities is challenging and even sometimes impossible. To gain understanding and allow comparison with theoretical predictions, laboratory-scale model systems such as Hele-Shaw (HS) cells are widely used. HS cells, two glass plates separated by a small gap, have the advantages of an easy direct visualization of the dynamics through the transparent walls and that the flow equations are equivalent, in some limit, to Darcy's law valid in real porous media (Homsy 1987). They have been extensively used for studies of vertical flows governed by the balance of buoyancy and viscous forces in vertical setups (Carballido-Landeira et al. 2013; Fernandez et al. 2002) or horizontal flows dominated by a balance of pressure and viscous forces (Homsy 1987; Maes et al. 2010). New life has been recently breathed into these studies on at least three fronts. First, the effects of chemical reactions on the flows have been taken into account showing that, for example, reactions can modify hydrodynamic instabilities and even destabilize otherwise stable flows (Loodts et al. 2014; Riolfo et al. 2012). Secondly, applications to enhanced petroleum recovery, horizontal drilling and fracturing, and carbon sequestration have focused researchers' efforts on attempts at controlling instabilities in porous flows (Al-Housseiny et al. 2012; Dias et al. 2010; Loodts et al. 2014;

Published online: 13 February 2016

Pihler-Puzović et al. 2012). Finally, advances in computational modeling and hardware have begun to provide information on the three-dimensional flow structure within the gap (Heussler et al. 2014; John et al. 2013; Oliveira and Meiburg 2011), and specifically on novel types of instabilities.

To compare theoretical predictions to experimental results, it is crucial to be able to monitor flow details in experiments in HS cells. Visualization is typically done by injecting a dyed fluid into a transparent fluid and recording the spatiotemporal evolution of the dye distribution with a camera (Fernandez et al. 2002; Haudin et al. 2014; Homsy 1987; Maes et al. 2010; Riolfo et al. 2012). However, particularly for low flow rates (small Péclet numbers), there is no guarantee that imaging the dye is equivalent to imaging the undyed fluid. This is all the more true for reactive systems where reactions can change locally the viscosity or density of the solutions (and hence the flow) at locations uncorrelated from the dye dynamics, as shown numerically (Nagatsu and De Wit 2011). In the case of reactive systems, chemical indicators such as pH indicators have also been used for visualization. However, these indicators have been shown to actively modify the flow in some cases (Almarcha et al. 2010b; Kuster et al. 2011; Thomas et al. 2015) and should, hence, be avoided if possible.

Other techniques have been used for imaging porous media flows (de Anna et al. 2014; Rose and Britton 2013; Wildenschild and Sheppard 2013). For HS cell dynamics, fluorescence (Bunton et al. 2014), shadowgraphy (Almarcha et al. 2010b), interferometry (Almarcha et al. 2010a, Grosfils et al. 2009), and Schlieren techniques have also been of growing interest. Schlieren imaging and related shadowgraph have been used extensively in numerous fields such as ballistics, wind-tunnel testing, combustion, and others (Settles 2001). Schlieren techniques have been usefully applied to noninvasively study both nonreactive (Carballido-Landeira et al. 2013) and reactive (Almarcha et al. 2011; Loodts et al. 2014) buoyancy-driven flows in vertical HS setups. Conceptually, the idea of the Schlieren technique is the same for both horizontal and vertical cases, i.e., the goal is to monitor deflection of light rays from a parallel beam due to flow dynamics in the cell. This involves a quite long optical bench to support all of the equipment starting from the light source to the recording camera via all intermediate lenses and the HS cell. This explains why, up until now, the technique has typically been used with vertical HS cells or for small-scale horizontal fields of view (Joannes et al. 2003). The situation is indeed trickier for larger fields of view in horizontal cells because it requires a very tall device. There is, however, interest in developing the method for such large-scale horizontal cases since the flow physics yields more complex three-dimensional dynamics than in vertical cells in which the flow is expected to be symmetric with respect to the vertical center plane of the HS cell.

In this context, we present here the development of a noninvasive optical method of Schlieren imaging to visualize fluid displacements along several centimeters in horizontal HS cells. We show that this technique allows visualization of the viscous flow dynamics, including 3D features, without the potential complications of interpretation posed by dyes and chemical indicators. Schlieren imaging also has an increased sensitivity over dyes, in some cases revealing internal features of flows difficult if not impossible to see with colorants. As an example, Fig. 1 shows fingers merging during a viscously unstable displacement of a glycerol solution by water, thus demonstrating the power of the technique to image the internal structure of the flow during a viscous fingering instability. In particular, a striped inner structure of the fingers due to a buoyancy-driven instability, as well as alignment of internal flows, can be followed during the merging. A comparison of experimental characteristics of these internal buoyancy-driven stripes with recent theoretical predictions shows the power gained by using the new Schlieren technique. We also show that additional qualitative information can be obtained on viscosity changes behind finger edges during reactive displacements.

The article is structured as follows: After presenting the details of implementation of the method, we show imaging of internal flows during unstable displacements of aqueous glycerol by water and in reactive fingering in a HS cell before discussing the comparison of the observed flow features with theoretical predictions and concluding.

2 Technique

Schlieren imaging dates back at least to the work of Toepler (Toepler 1864) and is described in depth in the book by Settles (Settles 2001). A basic understanding of the technique can be gained by referring to Fig. 2. First (Fig. 2—upper) broadband, white light emerges from a slit or pinhole, typically of dimensions a fraction of a millimeter. The light is collimated by a high-quality achromatic lens (L1) (Schlieren is often performed with off-axis mirrors in a "Z" configuration, but since lenses are used in the current context, that is the approach described herein). A second lens (L2 of focal length f_{L2}) refocuses the light forming an image of the slit or pinhole in its focal plane. A knife-edge or other cutoff (an iris in this work) is positioned at this focus so that it obstructs a portion of the light (generally speaking, obstructing more light increases sensitivity or contrast at the expense of dynamic range). At this point, the light that is unimpeded by the cutoff passes on to the focal plane of a camera where it forms a uniform background.

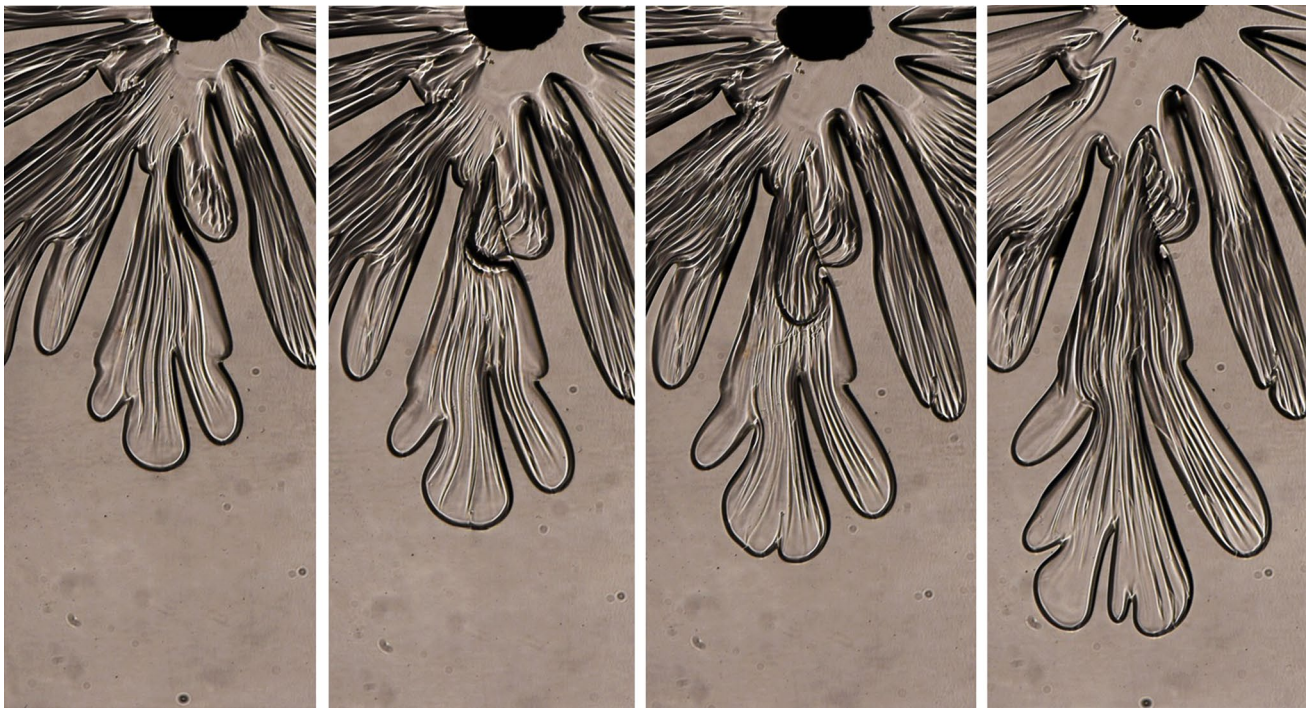

Fig. 1 Schlieren image of finger merging during injection of water into a more viscous aqueous solution of glycerol. The Schlieren images allow for following the dynamics both at the boundaries of the fingers and within the fingers, far behind their edges

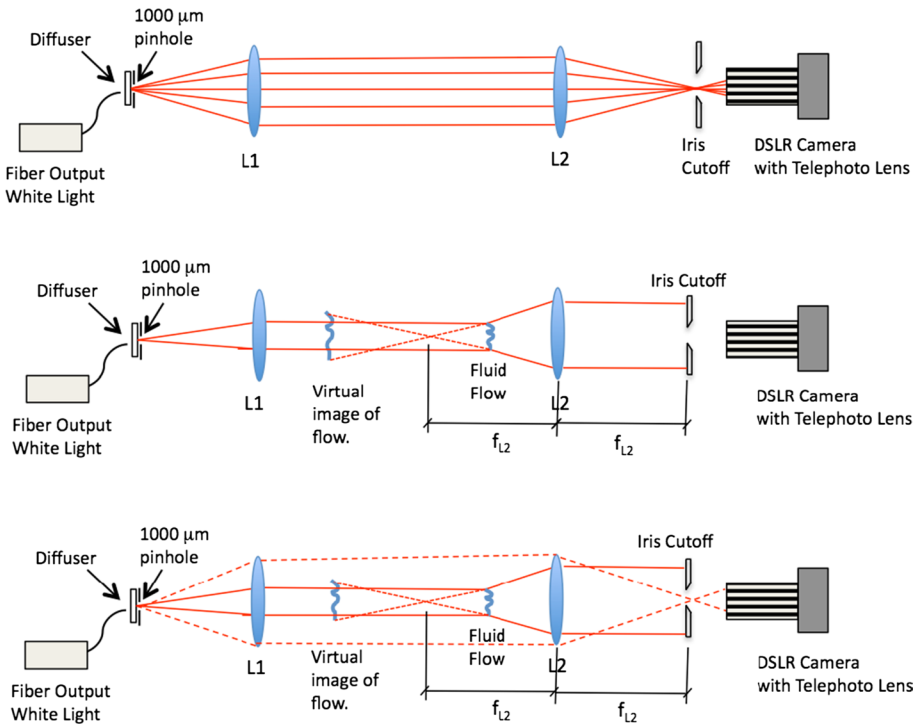

Fig. 2 Basics of Schlieren imaging as described in text

Referring now to Fig. 2 (middle), a transparent flow is introduced in some region along the collimated light path. For the configuration shown here, the flow must be closer to the final Schlieren lens than its focal length. The small change in index of refraction produced by the flow deflects some of the otherwise collimated light. Now, some light

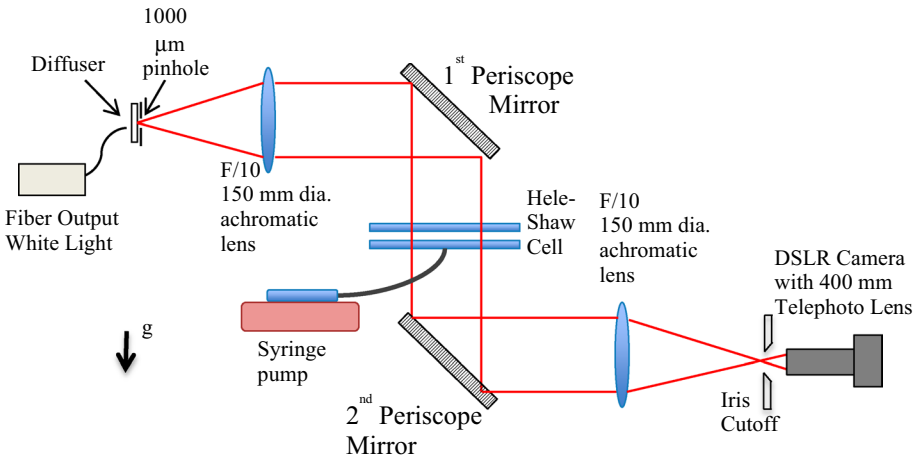

Fig. 3 *White* light from a pinhole is collimated by the first lens and then focused by the second. This forms an image of the slit at the second focal point of the second lens. The iris cutoff partially blocks this light, forming a *gray* background on the screen or focal plane of a camera. When a disturbance in the form of a fluid flow is introduced, the variation in index of refraction that results deflects a portion of the initially collimated beam. As a result, some light hits the iris that would otherwise have missed it and some misses the iris edge that would otherwise have hit it. This deviated light is available for forming an image. The second lens is positioned to form an image of the flow

strikes the cutoff that would otherwise have missed it and some misses it that would otherwise have hit it, thereby providing a source of contrast for image formation. Lens two forms a virtual image of the flow as shown in Fig. 2 (middle). A telephoto lens on the camera focuses through lens two onto the virtual image. Figure 2 (lower) shows the un-deflected light and the light deflected by the flow as well as its virtual image. Lenses used herein were F/10, 150 mm diameter, 1.5 m focal length achromatic telescope objective lenses obtained from Istar Optical. Lens mounts were custom-built in house.

In order to image horizontal flows in a HS cell, the classical Schlieren setup has been adapted: The new feature is that two periscope mirrors have been added to the system as seen in Fig. 3. All optics prior to the HS cell were elevated. A mirror oriented at 45° to the vertical directs the light down through the horizontal HS cell to a second mirror also oriented at 45° after which the light continues as usual. In earlier configurations, the optics prior to the HS cell were all at table height and two periscopes were used to direct the light up and over the cell and back down through it. While this approach did work and produced some beautiful images, it also introduced considerable astigmatism into the system. Elevating the initial optics and reducing the change in beam height to one periscope considerably reduced the astigmatism. Since astigmatism splits the focal point into two—the sagittal and tangential focus—it is a particularly troublesome aberration to deal with in a Schlieren system where the system focus plays such a key role. The Schlieren system is shown in Fig. 4.

In principle, one could use lower f-number and therefore shorter focal length, achromatic objective lenses. However, in practice, this would have resulted in unacceptable optical aberrations for the desired 12-cm field of view. A relative aperture of f/10 or more is recommended for the two primary Schlieren lenses. Furthermore, sensitivity increases with focal length in Schlieren imaging. Hence, as is often done in Schlieren of larger objects, the object—the flow in this case—was moved closer than one focal length to the second Schlieren lens. This results in a virtual image being formed on the flow side of the second Schlieren lens (that is, before it) somewhere between the focal length and infinity. That is, the second lens is acting as a simple magnifier. A telephoto zoom lens must be used to look through the second lens and focus on the virtual image. The current system uses an 80–400-mm Nikkor f/4.5-5.6G lens on a Nikon D810 camera with a 36-megapixel sensor. However, quite acceptable images can be obtained with lower-cost camera and telephoto lens. Since the system described herein uses two 1.5 m focal length lenses, fourfold mirrors were necessary for the system to fit on a 1.2 m × 2.4 m optical table. This also undoubtedly introduces aberrations, and a straight-line system would be an improvement in principle. However, in practice, the images obtained are more than acceptable.

Traditional Schlieren uses a knife-edge or razor at the system focus; however, this is not the only approach. Four "cut off" techniques were tested providing varying degrees of success. One was to image without any razor at all. This presumably uses the naturally occurring apertures in the system as the cutoff such as the Schlieren mirrors or

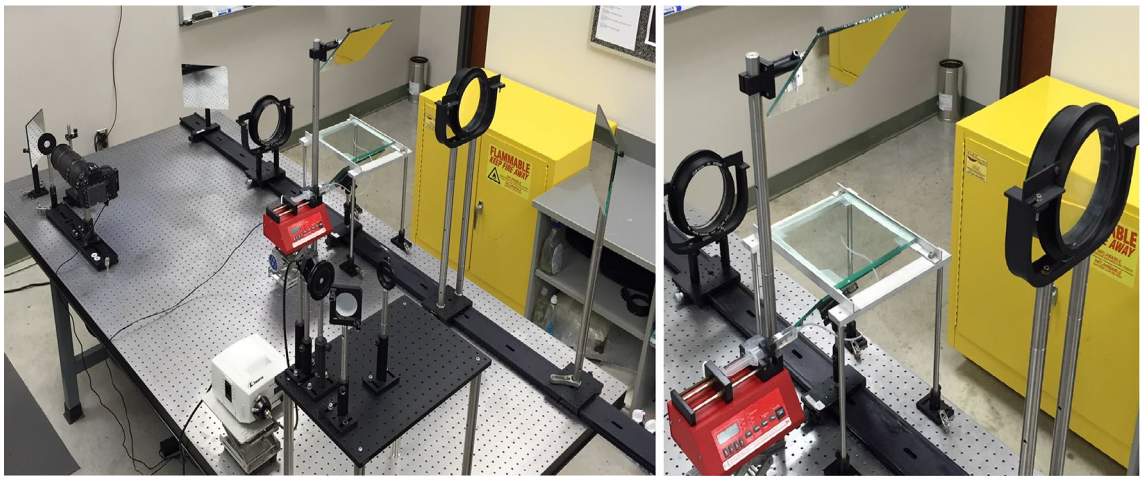

Fig. 4 (*Left*) Schlieren imaging system described herein. (*Right*) Schlieren lenses, periscope, HS cell, and syringe pump

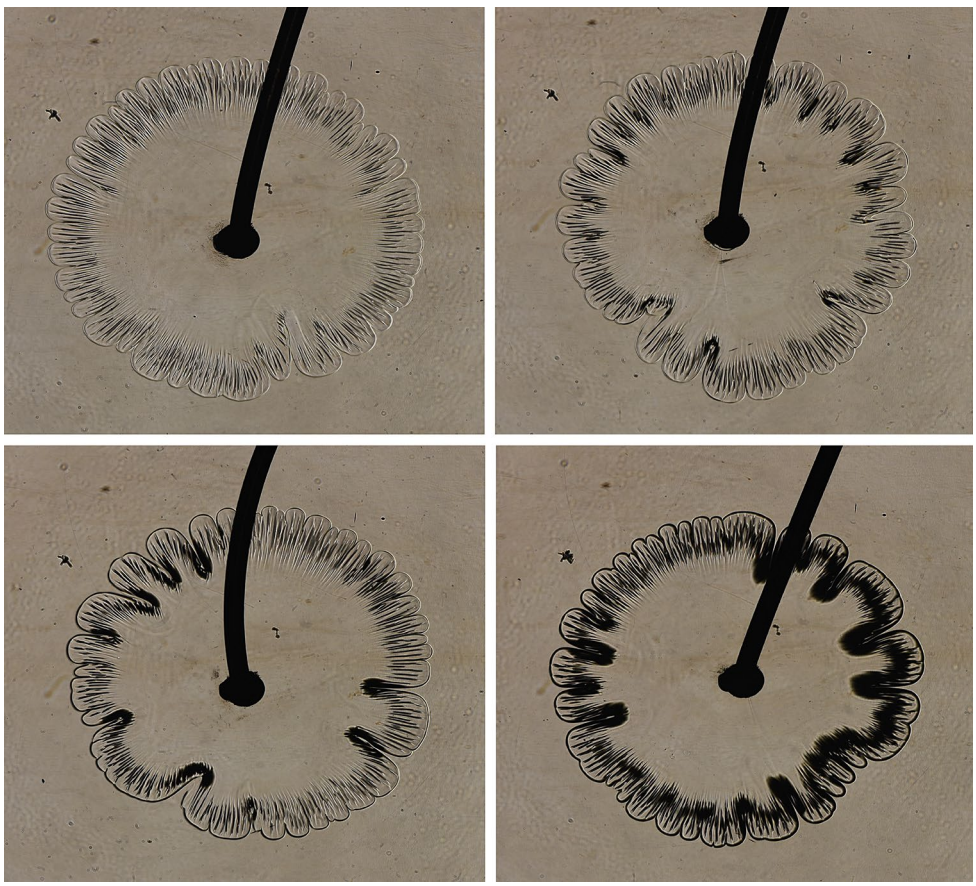

Fig. 5 Water displacing a 65 % glycerol–water solution with increasing contrast achieved by stopping down iris at system focus in front of the camera lens. *Upper left* 39 mm iris. *Upper right* 26 mm iris. *Lower left* 18 mm iris. *Lower right* 13 mm iris. Note that use of the iris increases contrast at the interface between the two fluids but at the expense of detail. (Images are from different flows 35 s after start of flow. Flow parameters were 1.00 mL/min, 0.35 mm gap. Brightness of images was increased by 20 % in postprocessing to aid in viewing). Field of view: 7.4 cm x 6.6 cm

aperture(s) in the telephoto lens. For flows with comparatively large index gradients, this is not only sufficient, but also actually works quite well, as introducing an additional cutoff can overly darken the image. Secondly, a razor was used as a knife-edge at the system focus. Despite best efforts, this consistently resulted in a darkening of one side of the image as compared to the other. This is presumably due to aberrations introduced by the periscope and fold mirrors. In passing, both a slit and a pinhole were tried at the source focus with a pinhole ultimately being preferred. Third, an iris was positioned as the cutoff in the system focus.

Stopping the iris down increases sensitivity, as discussed below in connection with Fig. 5. This also eliminated the

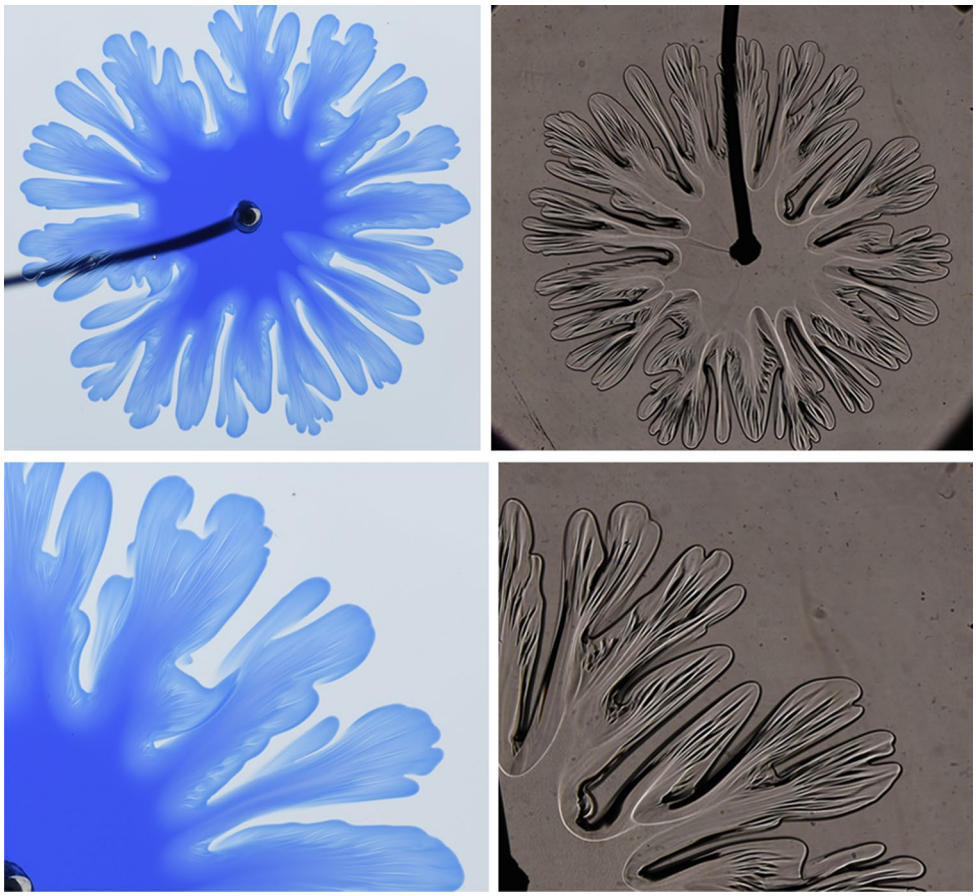

Fig. 6 Comparison of dye and Schlieren imaging of viscous fingering developing when water is injected into 80 % glycerol at 2.00 mL/min for a 0.35-mm gap in the HS cell. *Left* (*upper* and *lower*) Imaged using 0.06 % trypan blue dye in water. *Right* (*upper* and *lower*) Imaged using Schlieren. Note the increased clarity of the internal flows in the Schlieren image, which simplifies counting of the internal stripes for wavelength determination. (Brightness of Schlieren images was increased by 20 % in postprocessing to aid in viewing)

preferential darkening of one side of the image. Finally, a zero-order stop was introduced by blocking the middle of the beam at the system focus with a circular spot on a microscope slide. This is based on the Fourier optics result that the Fourier transform of an object plane is produced in the focal plane of a lens system (Meyer-Arendt 1995). The low spatial frequencies pass through the focal plane near the axis, and the higher spatial frequencies (the edge information) off axis. Thus, blocking some of the on-axis light in the final focal plane eliminates background light while preserving the light that carries the information. This works well; however, it is difficult to adjust contrast. Ultimately, an iris was used because of benefits of easily adjustable contrast as well as elimination of the preferential darkening that occurred with the knife-edge. Note that more than one of the techniques can be used simultaneously, and some trial and error may be appropriate to determine the best technique(s) for a given flow. Figure 5 shows similar flows imaged with decreasing iris aperture. The contrast increases for decreasing aperture at the expense of detail. The ability to adjust contrast and sensitivity is an additional benefit of Schlieren imaging over more traditional dye systems. Of course digital image enhancement can be used to further increase contrast, but this was not done here to clearly demonstrate the technique (however, the image was brightened in postprocessing for ease of viewing).

Figure 6 compares dye and Schlieren imaging of identical systems of water displacing a more viscous 80 % glycerol–water solution at 2.00 mL/min in a horizontal HS cell with a 0.35-mm gap. The dyed system used 0.06 % trypan blue dissolved in water. The Schlieren image shows greater contrast and clarity of features. Schlieren imaging is much more tunable than dye imaging since (1) adjusting the cutoff controls sensitivity and dynamic range, and (2) multiple techniques can be combined such as a zero-order stop and Schlieren to search for features in the flow. On the other hand, the techniques may also be considered complimentary. For example, in the lower left-hand image of Fig. 6, lighter colors presumably correspond to the undyed, displaced fluid (aqueous glycerol in this case). Schlieren (and related techniques) cannot distinguish which fluid is causing an internal feature but is only sensitive to index of refraction gradients. Dye imaging can also be adjusted to some degree by adjusting the intensity of the backlight to take advantage of more of the dynamic range of the camera. Having said this, however, over long times, one must always bear in mind that dye imaging is just

that—imaging the dye. Dye diffusion or dispersion may or may not be representative of the pure system. No such complication emerges in Schlieren.

Schlieren imaging of horizontal systems can also be very useful for analyzing reactive flows as seen in Fig. 7, where a dithiol monomer with initiator is displacing a diacrylate monomer (specifically 2,2′-(ethylenedioxy) diethanethiol (herein "dithiol") containing 1,8-diazabicycle[5.4.0]undec-7-ene (herein "DBU") displacing poly(ethylene glycol)diacrylate average Mn = 575) (herein "PEG 575″). The darker regions correspond to increased polymer conversion. On the left, no initiator is present; consequently, the two fluids do not react. The only difference for the flow on the right was the addition of an initiator to the dithiol so that the two monomers react by step-growth polymerization to form a linear polymer. The darker regions correspond to increased polymer conversion and therefore increased viscosity. For the case shown, the reaction is seen to trail behind the VF front. The highest degree of reaction is occurring between the fingers, while less reacted fluid is clearly seen to extend behind the fingers. Information on such viscosity changes behind the edge of the fingers is impossible to obtain with dyes (Loodts et al. 2014; Riolfo et al. 2012).

3 Results and discussion

The Schlieren imaging system described herein has been used to study miscible viscous fingering in glycerol–water systems in a horizontal HS cell. Experimental investigations of miscible fingering in HS cells have a long history, dating back to the seminal work by Wooding (Wooding 1969). For a review of this research area, we refer the reader to Oliveira and Meiburg (2011). These authors employ three-dimensional Stokes simulations to explore miscible displacements of a more viscous fluid by a less viscous one, in the absence of density differences.

In the Stokes regime, and in the absence of density differences, such flows are governed by the viscosity ratio M and the Péclet number Pe. These dimensionless parameters are defined as

$$M = \frac{\mu_2}{\mu_1}, \quad \mathrm{Pe} = \frac{Ue}{D} \tag{1}$$

Here μ_2 (μ_1) denotes the viscosity of the displaced (displacing) fluid. U represents the injection speed, e indicates the gap width of the HS cell, and D is the diffusion coefficient of glycerol into water. For rectilinear displacements, quasi-steady fingers can form (Fig. 8), whose tip velocity increases with the Péclet number and the viscosity ratio (Oliveira and Meiburg 2011). In addition to the well-known tip-splitting instability, these fingers are seen to give rise to a streamwise vorticity quadrupole, which convects resident fluid from the wall to the center of the gap, while it transports injected fluid laterally away from the finger center within the mid-gap plane. In this way, the streamwise vorticity quadrupole results in the emergence of a longitudinal, inner splitting phenomenon some distance behind the fingertip. While this inner splitting instability had not been previously reported in the literature, closer inspection of

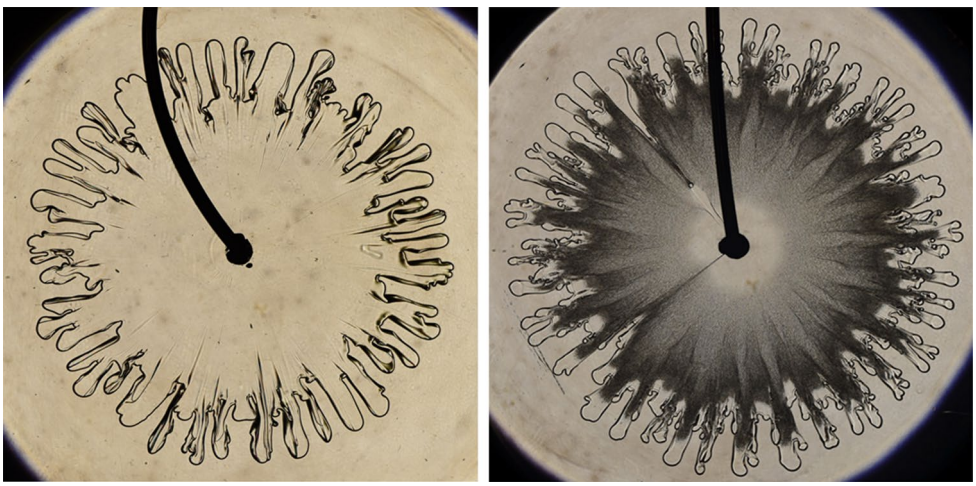

Fig. 7 Schlieren images comparing unreactive and reactive viscous fingering. In both cases, a dithiol monomer is displacing a diacrylate monomer. *Left* No initiator of the polymerization reaction is present, so the two fluids do not react. *Right* Identical flow parameters except that initiator are added to the dithiol, so that the two monomers react by step-growth polymerization to form a linear polymer. The *darker* regions correspond to increased polymer conversion. The reaction is seen here to trail behind the viscous fingering front. Field of view: 13 cm diameter

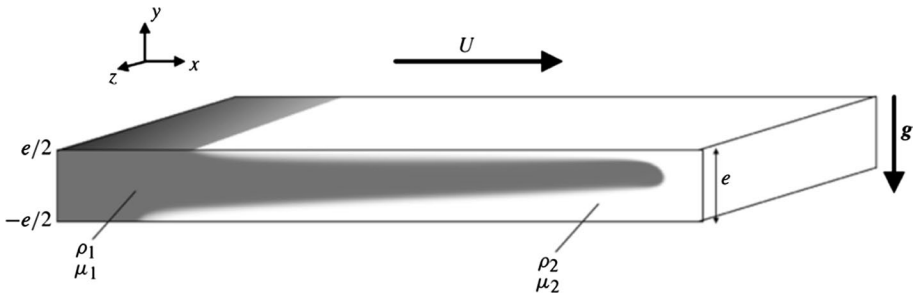

Fig. 8 Schematic of a less viscous fluid displacing a more viscous one (possibly of different density) in a horizontal HS cell taken from the stability analysis of Talon et al. (2013)

the figures of Wooding (1969) confirms its existence in those early experiments.

The simulation work (Oliveira and Meiburg 2011) was next extended to horizontal displacements with density differences (cf. Fig. 8) (John et al. 2013). The density difference between the displacing and displaced fluids gives rise to an additional dimensionless parameter F defined as

$$F = \frac{\Delta\rho g e^2}{\mu_2 U} \tag{2}$$

where $\Delta\rho = \rho_2 - \rho_1$ denotes the density difference, with ρ_1 (ρ_2) the density of the displacing (displaced) fluid. Depending on the sign of the density difference between the two fluids, either the upper or the lower interface between the injected fluid propagating along the center of the gap and the resident fluid next to the wall becomes gravitationally unstable (if the fluids were immiscible, with a surface tension force acting along the interface, F could be interpreted as the ratio of suitably defined Bond and capillary numbers). This density-driven instability

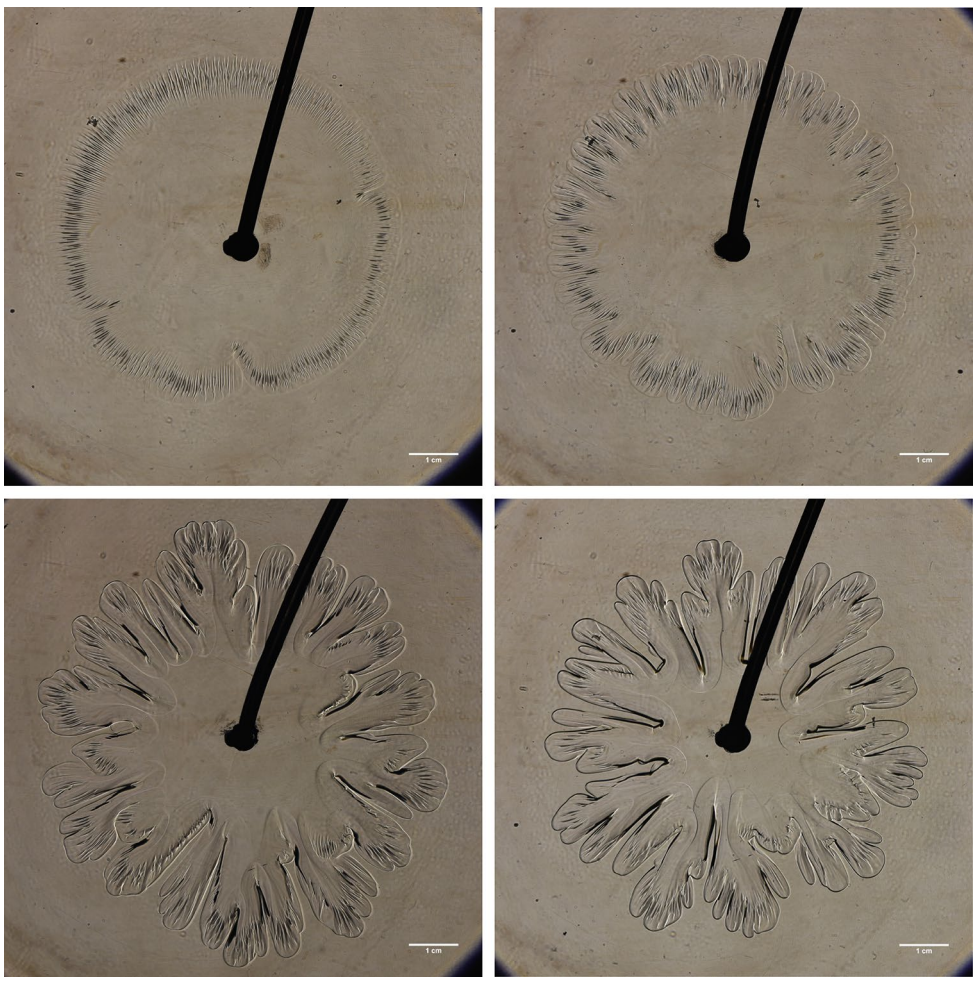

Fig. 9 Water flowing into various aqueous solutions of glycerol, all at 1 mL/min and 0.35 mm gap. *Upper left* 55 % glycerol. *Upper right* 65 % glycerol. *Lower left* 80 % glycerol. *Lower right* 85 % glycerol. Contrast and brightness were increased by 20 % in post-processing to aid in viewing. Field of view: 9 cm x 9 cm

results in the formation of thin little stripes developing in the invading fluid and perpendicular to the front, as seen using a dye in a viscously stable case (Haudin et al. 2014). These stripes result from streamwise, counter-rotating vortices, such as can be seen in Figs. 10 and 20 in John et al. (2013). Talon et al. (2013) conducted a detailed linear stability analysis of this density-driven instability. By performing a parametric investigation, they find that the dominant spanwise wavelength of these streamwise vortices typically lies between one half and one full gap width, which is consistent with the nonlinear simulation results of John et al. (2013) (compare their Figs. 10 and 20).

Figure 9 shows Schlieren images of water flowing into various aqueous solutions of glycerol, in a radial HS cell. Radial HS displacements share many features with rectilinear displacements, but there are also a few notable differences. Chief among them is the decay of the displacement front velocity with time in the radial displacement. The images clearly demonstrate both the well-known viscous fingering instability of the displacement front, and narrowly spaced radial streaks behind the front that are associated with the gravitational instability mode investigated by Haudin et al. (2014), Talon et al. (2013), and John et al. (2013). Figure 10 shows a close-up image of water displacing 20 % glycerol–water solution. It serves as an excellent example of the clarity of imaging achievable with Schlieren. The inner streamwise vortices are easily seen as well as their splitting and their formation behind the front between the displacing and displaced fluids. Table 1 lists the experiments conducted as part of the present investigation, along with the corresponding values of M, Pe and F, and the resulting spacing between the radial streaks observed in the images. As several ranges of diffusion coefficient for glycerol–water systems exist in the literature (Petitjeans and Maxworthy 1996; Ternström et al. 1996), we use here the representative value $D = 6 \times 10^{-10}$ m^2/s to compute the Pe number. As the percentage of glycerol increases, the viscosity of the defending fluid increases exponentially. Viscosities of glycerol–water solutions were taken from *Glycerol* (Newman 1968). Linear interpolation was used where necessary to account for varying temperatures and/or concentrations. The viscosity ratio M is varied by over an order of magnitude (from approximately 10 to 100). Hence, the intensity of the fingering instability at the displacement front increases, and its azimuthal wavelength decreases. What is pertinent here is how Schlieren is capable of imaging the smaller features associated with the radial streaks internal to the primary fingers. Using

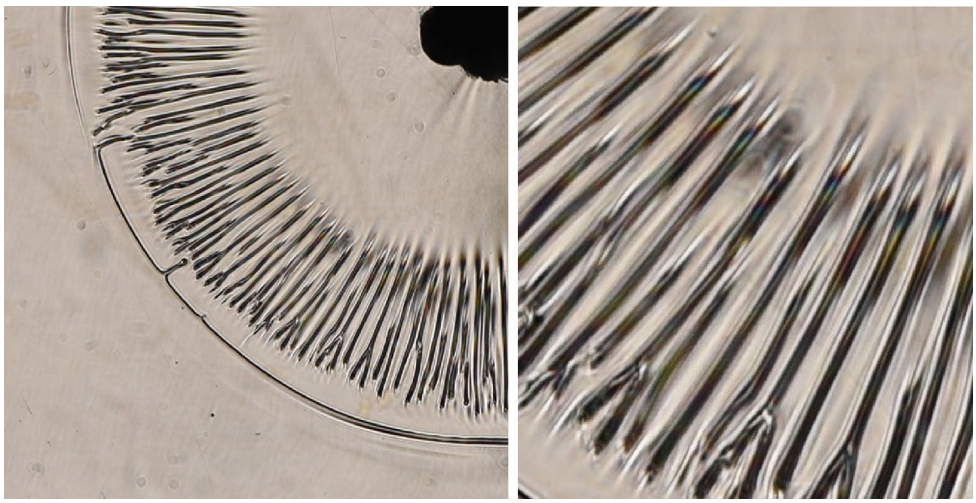

Fig. 10 (*Left*) water displacing 20 % glycerol–water solution at 1.857 mL/min flow rate and a gap of 0.65 mm. The little stripes corresponding to the counter-rotating flows predicted in the literature are easily visible (as well as their splitting). Furthermore, they are seen to form behind the front as predicted. (*Right*) zoom in on region of same image. Roots of stripes may suggest that each stripe is actually a pair of counter-rotation vortices

Table 1 Varying concentrations of glycerol and associated parameters

% Glycerol (by mass)	T (°C)	$\Delta\rho$ (kg/m^3)	$\mu_{glycerol}$ (N s/m^2)	μ_{water} (N s/m^2)	υ (m/s)	Experimental wavelengths				M	Pe	F
						Half-time λ (10^{-3} m)	Half-time λ/b (10^{-3} m)	Minimum λ (10^{-3} m)	Minimum λ/b (10^{-3} m)			
55	21.5	141.8	0.008	0.000947	6.48E−04	0.960	2.7	0.744	2.1	8.4	380	33
65	20.5	168.8	0.015	0.000995	6.71E−04	0.872	2.5	0.608	1.7	15	390	20
80	21.5	209.8	0.056	0.000947	7.87E−04	1.27	3.6	1.086	3.1	59	460	5.7
85	22.0	224.2	0.099	0.000964	7.38E−04	1.52	4.3	1.53	4.4	100	430	3.7

dye imaging on a viscously stable displacement, Haudin et al. (2014) have shown that the small fingers in the 55 % glycerol system are attributable to a gravitational instability due to layering induced by the Poiseuille profile. These are readily observed at the periphery of the 55 and 65 % flows. They are further observable at the ends of the primary fingers in the higher glycerol concentrations with correspondingly higher viscosity. In the present viscously unstable experiments, the density parameter F also varies roughly over one order of magnitude, from 3.7 to 33. The Péclet number remains nearly constant in the experiments, in the range of O(400). Of course F and Pe vary during the course of the experiment since for radial flows the front velocity is constantly decreasing. A representative value for U was used in computing them, determined by taking the maximum flow radius and dividing by the flow time. This naturally underestimates initial flow front velocities and overestimates the final values.

When comparing the experimentally observed wavelengths of the gravitational instability to the theoretical predictions by Talon et al. (2013), and to the simulation data of John et al. (2013), a few key differences between the respective setups need to be kept in mind. First of all, the linear stability analysis (Talon et al. 2013) and the simulations (John et al. 2013) were performed for rectilinear displacements, which are characterized by a unidirectional base flow velocity that is constant in space and time. The present experiments, on the other hand, were conducted in radial HS cells. Here the displacement velocity varies inversely proportional to the radius, so that the radial velocity of the displacement front is time dependent. Furthermore, the direction of the base flow velocity depends on the azimuthal angle, which results in the continuous stretching of the displacement front. Hence, it would appear likely that an emerging, small amplitude azimuthal perturbation of a certain wavelength will be stretched azimuthally as it is convected along with the base flow, so that its wavelength will continuously increase from the initial value at which the instability first emerged, at least until such time as it splits after which the azimuthal stretching continues anew. The wavelength data listed in Table 1 are consistent with these considerations. Specifically, they indicate a trend toward smaller wavelengths for larger values of F, in agreement with the linear stability results shown in Figure 21 of Talon et al. (Talon et al. 2013). Note that the wavelengths in Table 1 are computed as twice the distance between the stripes in the experimental data since there are two counter-rotating vortices per wavelength, but each vortex could show up in Schlieren. Since the wavelength varies with radius, reasonable choices had to be made as to where to measure. Two such choices are shown in Table 1. The experimental minimum wavelength is the wavelength as measured in the earliest image where the streaks were clearly observable. The "half time" wavelength was measured using the image corresponding to when the flow was half over. This choice better corresponds to the velocity estimate used in computing F and Pe. At the smallest radii where the azimuthal instability can first be visually detected, the ratio of the wavelength to the gap width varies between 1.7 and 4.4, whereas for the half-time radii this ratio varies from 2.5 to 4.3. While these values are somewhat larger than those of O(1) predicted theoretically for rectilinear displacements, in light of the above discussion of the differences between experiments and theory, the agreement can be considered satisfactory. It may be that each stripe is actually a pair of counter-rotating vortices. If one zooms in on the roots of the stripes as in Fig. 10 (right), there is some suggestion this may be the case. If so, then this would bring the experiment and theory into even closer agreement.

4 Conclusion

We have introduced here an adaptation of a Schlieren imaging technique including the addition of two periscope mirrors to allow analyzing flow dynamics in a horizontal HS cell. The technique has been applied to monitor flow details during viscously unstable displacement of nonreactive and reactive fluids. The main advantages of the method with regard to dye imaging are its increased sensitivity to detect flow details and the possibility of obtaining information on the dynamics *inside* each fluid zone. In particular, it can monitor dynamics in the invading fluid well behind the edge of the fingers, a zone classically difficult to study when colored by a dye.

To demonstrate the efficiency of our adapted Schlieren technique in the study of flow displacement, we have shown internal flow details in the invading fluid in the cases of finger merging, reactive displacements, and buoyancy-driven instabilities inside fingers. In this latter case, we have made a clear identification and quantitative characterization of azimuthally periodic structures in the radial direction attributed to gravitational instabilities. The azimuthal wavelengths observed here are consistent with those investigated earlier theoretically for rectilinear displacements.

Acknowledgments We thank Macy Tush for assisting with data collection and John Pojman of the Louisiana State University for proposing the reactive step-growth polymerization system. P.B. acknowledges support of the National Science Foundation Grant CBET-1335739. A.D. thanks Prodex and FRS-FNRS under the FORECAST project for financial support. E.M. acknowledges support through NSF Grant CBET-0651498.

References

Al-Housseiny TT, Tsai PA, Stone HA (2012) Control of interfacial instabilities using flow geometry. Nat Phys 8:747–750

Almarcha C, Trevelyan PMJ, Grosfils P, De Wit A (2010a) Chemically-driven hydrodynamic instabilities around A + B → C fronts. Phys Rev Lett 104:044501

Almarcha C, Trevelyan PMJ, Riolfo LA et al (2010b) Active role of color indicators in buoyancy-driven instabilities of chemical fronts. J Phys Chem Lett 1:752–757

Almarcha C, R'Honi Y, De Decker Y, Trevelyan PMJ, Eckert K, De Wit A (2011) Convective mixing induced by acid-base reactions. J Phys Chem B 115:9739–9744

Bunton P, Dice B, Pojman JA, De Wit A, Brau F (2014) Quantitative viscosity field reconstruction of Hele-Shaw flows by imaging fluorescent molecular probes. Phys Fluid 26:114106

Carballido-Landeira J, Trevelyan PMJ, Almarcha C, De Wit A (2013) Mixed-mode instability of a miscible interface due to coupling between Rayleigh–Taylor and double-diffusive convective modes. Phys Fluids 25:024107

de Anna P, Jimenez-Martinez J, Tabuteau H et al (2014) Mixing and reaction kinetics in porous media: an experimental pore scale quantification. Environ Sci Technol 48:508–516

Dias E, Parisio F, Miranda J (2010) Suppression of viscous fluid fingering: a piecewise-constant injection process. Phys Rev E 82:067301

Fernandez J, Kurowski P, Petitjeans P, Meiburg E (2002) Density-driven unstable flows of miscible fluids in a Hele-Shaw cell. J Fluid Mech 451:239–260

Grosfils P, Dubois F, Yourassowsky C, De Wit A (2009) Hot spots revealed by simultaneous experimental measurement of the two-dimensional concentration and temperature fields of an exothermic chemical front during finger-pattern formation. Phys Rev E 79:017301

Haudin F, Riolfo LA, Knaepen B, Homsy GM, De Wit A (2014) Experimental study of a buoyancy-driven instability of a miscible horizontal displacement in a Hele-Shaw cell. Phys Fluids 26:044102

Heussler F, Oliveira R, John M, Meiburg E (2014) Three-dimensional Navier–Stokes simulations of buoyant, vertical miscible Hele-Shaw displacements. J Fluid Mech 752:157–183

Homsy GM (1987) Viscous fingering in porous media. Ann Rev Fluid Mech 19:271–311

Joannes L, Dubois F, Legros J (2003) Phase-shifting schlieren: high-resolution quantitative schlieren that uses the phase-shifting technique principle. Appl Opt 42:5046–5053

John MO, Oliveira RM, Heussler FHC, Meiburg E (2013) Variable density and viscosity, miscible displacements in horizontal Hele-Shaw cells. Part 2. Nonlinear simulations. J Fluid Mech 721:295–323

Kuster S, Riolfo LA, Zalts A et al (2011) Differential diffusion effects on buoyancy-driven instabilities of acid-base fronts: the case of a color indicator. Phys Chem Chem Phys 13:17295–17303

Loodts V, Thomas C, Rongy L, De Wit A (2014) Control of convective dissolution by chemical reactions: general classification and application to CO_2 dissolution in reactive aqueous solutions. Phys Rev Lett 113:114501

Maes R, Rousseaux G, Scheid B, Mishra M, Colinet P, De Wit A (2010) Experimental study of dispersion and miscible viscous fingering of initially circular samples in Hele-Shaw cells. Phys Fluids 22:123104

Meyer-Arendt JR (1995) Introduction to classical and modern optics. Prentice Hall, Englewood Cliffs

Nagatsu Y, De Wit A (2011) Viscous fingering of a miscible reactive A + B → C interface for an infinitely fast chemical reaction: nonlinear simulations. Phys Fluids 23:043103

Newman AA (1968) Glycerol. C. R. C. Press, Cleveland

Oliveira RM, Meiburg E (2011) Miscible displacements in Hele-Shaw cells: three-dimensional Navier–Stokes simulations. J Fluid Mech 687:431–460

Petitjeans P, Maxworthy T (1996) Miscible displacements in capillary tubes. Part 1. Experiments. J Fluid Mech 326:37–56

Pihler-Puzović D, Illien P, Heil M, Juel A (2012) Suppression of complex fingerlike patterns at the interface between air and a viscous fluid by elastic membranes. Phys Rev Lett 108:074502

Riolfo LA, Nagatsu Y, Iwata S, Maes R, Trevelyan PMJ, De Wit A (2012) Experimental evidence of reaction-driven miscible viscous fingering. Phys Rev E 85:015304

Rose HEL, Britton MM (2013) Magnetic resonance imaging of reaction-driven viscous fingering in a packed bed. Microporous Mesoporous Mater 2013:64–68

Settles GS (2001) Schlieren and shadowgraph techniques. Springer, Berlin

Talon L, Goyal N, Meiburg E (2013) Variable density and viscosity, miscible displacements in horizontal Hele-Shaw cells. Part 1: linear stability analysis. J Fluid Mech 721:268–294

Ternström G, Sjöstrand A, Aly G, Jernqvist Å (1996) Mutual diffusion coefficients of water + ethylene glycol and water + glycerol mixtures. J Chem Eng Data 41:876–879

Thomas C, Lemaigre L, Zalts A, D'Onofrio A, De Wit A (2015) Experimental study of CO_2 convective dissolution: the effect of color indicators. Int J Greenh Gas Control 42:525–533

Toepler A (1864) Beobachtungen nach einer neuen optischen Methode - Ein Beitrag zur Experimentalphysik. M. Cohen & Son, Bonn

Wildenschild D, Sheppard A (2013) X-ray imaging and analysis techniques for quantifying pore-scale structure and processes in subsurface porous medium systems. Adv Water Resour 51:217–246

Wooding RA (1969) Growth of fingers at an unstable diffusing interface in a porous medium or Hele-Shaw cell. J Fluid Mech 39:477–495